Proceedings of FEDSM '01
2001 ASME Fluids Engineering Conference
May 29 - June 1, 2001, New Orleans, Louisiana

FEDSM2001-18114

PERFORMANCE ANALYSIS OF CAVITATING FLOW IN CENTRIFUGAL PUMPS USING MULTIPHASE CFD

Richard B. Medvitz*, **Robert F. Kunz**†, **David A. Boger, Jules W. Lindau, Adam M. Yocum**
Applied Research Laboratory
The Pennsylvania State University
University Park, Pennsylvania 16804
814-863-7139, rbm120@psu.edu

Laura L. Pauley‡
Department of Mechanical Engineering
The Pennsylvania State University
University Park, Pennsylvania 16802

ABSTRACT

A multi-phase CFD method is used to analyze centrifugal pump performance under developed cavitating conditions. The differential model employed is the homogeneous two-phase Reynolds-Averaged-Navier-Stokes equations, wherein mixture momentum and volume continuity equations are solved along with vapor volume fraction continuity. Mass transfer modeling is provided for the phase change associated with sheet cavitation. Quasi-three-dimensional (Q3D) and fully-three-dimensional analyses are performed for two impeller configurations. Using Q3D analysis, steady and time-dependent analyses were performed across a wide range of flow coefficients and cavitation numbers. Characteristic performance trends associated with off-design flow and blade cavitation are observed. The rapid drop in head coefficient at low cavitation numbers (breakdown) is captured for all flow coefficients. Local flow field solution plots elucidate the principal physical mechanisms associated with the onset of breakdown. Results are also presented which illustrate the full three dimensional capability of the method.

1 Introduction

Cavitation physics play an important role in the design and operation of many liquid handling turbomachines. In particular, cavitation can give rise to erosion damage, noise, vibration and hydraulic performance deterioration. Accordingly, a large body of research has been performed towards understanding the physics of, designing away from, and designing to accommodate the effects of cavitation.

In many pump applications, large scale developed, or "sheet" cavities form on the blade and endwall surfaces when the pump operates off design flow or at low system pressure. In addition to erosion and noise implications, if these cavities become large, they exhibit significant unsteadiness and can vary significantly in extent from blade to blade. These effects conspire to generate potentially damaging vibration due to non-uniform loading around the annulus. Additionally, for low enough cavitation numbers, hydraulic efficiency, flow coefficient and head coefficient can decrease. Ultimately, cavitation breakdown can occur as characterized by a very rapid decrease in impeller head rise coefficient. For these reasons, it is of interest to the pump designer to be able to model large scale cavitation.

Potential flow methods have been employed for decades to model large cavities in a variety of liquid flow systems including pumps. These methods treat the fluid flow outside the bubble as potential flow, while the shape and size of the bubble itself are determined from dynamic equilibrium assumptions across the bubble-liquid interface, with bubble shape family and/or closure conditions also provided. Adaptations of such methods remain in widespread use today due to their inherent computational efficiency, and their proven effectiveness in predicting numerous first

* Graduate Research Assistant
† Research Associate, Thesis Co-advisor
‡ Associate Professor, Thesis Co-advisor

order dynamics of sheet- and super-supercavitating configurations, but they retain the limitations of a potential flow model applied to a flow with complex bubble geometries and inherent vortical structures. Recently, more general CFD approaches have been developed to analyze these flows. In the pump application area, Hirschi et al. [4] employed a single-phase RANS methodology wherein the cavity boundary is treated as a constant pressure slip surface, with the cavity geometry defined from bubble dynamics and closure condition modeling. In the past several years several research groups ([1], [2], [10], [13], for example) as well as commercial CFD vendors have introduced large scale cavitation models (for pumps and other applications) wherein the entire flow path is treated using the same differential model, with phase change incorporated to account for the generation and condensation of the cavitation bubble. This is the approach taken here.

In particular, the authors have recently developed a multiphase CFD methodology with applications focused on sheet- and super-cavitating flows about underwater vehicles [6-9]. As this capability has been matured and validated for that class of applications, we have begun to pursue developed cavitation in turbomachinery. This paper summarizes our capabilities and results in this area to date.

The paper is organized as follows: The theoretical formulation of the method is briefly summarized, including baseline differential model, specific physical models and numerical methods. This is followed by two sets of results. First, Q3D analyses are presented for a 7-blade impeller operating across a range of flow coefficients and cavitation numbers. Analyses are also presented which illustrate the fully 3D capability of the method.

2 Nomenclature

Symbols

c	blade chord length
C_μ, C_{dest}, C_{prod}	turbulence and mass transfer model constants
k	turbulence kinetic energy
$\dot{m}^-$, $\dot{m}^+$	mass transfer rates
p	pressure
Re	Reynolds number
t, t_∞	time, mean flow time scale (c/U_{tip})
$\vec{T}$	total torque exerted by blade
U_{tip}	blade tip speed
u_i	Cartesian velocity components
V^2_{ref}	reference velocity ($U^2_{tip} + V^2_{x,\,inlet}$)
x_i	Cartesian coordinates
α	volume fraction
β	preconditioning parameter
ε, ε_{ijk}	turbulence dissipation rate, permutation tensor
η	pump hydraulic efficiency
θ	angular coordinate
μ	molecular viscosity
ρ	density
σ	cavitation number
τ	pseudo-time
ϕ	flow coefficient
ψ	head coefficient
ω_i	machine angular velocity

Subscripts, Superscripts

i, j, k, l, m	Cartesian tensor indices
l	liquid
m	mixture
t	turbulent
v	vapor

3 Theoretical Formulation

Governing Equations and Physical Modeling

A two-phase differential formulation is adopted where individual equations are provided for the transport, generation and destruction of volume fraction of liquid (which can exchange mass with vapor), and the mixture volume. A mixture momentum equation is also provided. The governing differential equations, cast in Cartesian tensor form, in a frame of reference rotating with constant angular velocity, ω_i, are given as:

$$\left(\frac{1}{\rho_m\beta^2}\right)\frac{\partial p}{\partial\tau}+\frac{\partial u_j}{\partial x_j} = (\dot{m}^+ + \dot{m}^-)\left(\frac{1}{\rho_l}-\frac{1}{\rho_v}\right)$$

$$\frac{\partial}{\partial t}(\rho_m u_i)+\frac{\partial}{\partial\tau}(\rho_m u_i)+\frac{\partial}{\partial x_j}(\rho_m u_i u_j) = -\frac{\partial p}{\partial x_i}+$$

$$\frac{\partial}{\partial x_j}\left(\mu_{m,t}\left[\frac{\partial u_i}{\partial x_j}+\frac{\partial u_j}{\partial x_i}\right]\right)-\rho_m\varepsilon_{ijk}\omega_j\varepsilon_{klm}\omega_l x_m-\rho_m 2\varepsilon_{ijk}\omega_j u_k \qquad (1)$$

$$\frac{\partial\alpha_l}{\partial t}+\left(\frac{\alpha_l}{\rho_m\beta^2}\right)\frac{\partial p}{\partial\tau}+\frac{\partial\alpha_l}{\partial\tau}+\frac{\partial}{\partial x_j}(\alpha_l u_j) = \left(\frac{\dot{m}^+}{\rho_l}+\frac{\dot{m}^-}{\rho_l}\right)$$

where mixture density and turbulent viscosity are defined by:

$$\rho_m = \rho_l\alpha_l + \rho_v\alpha_v, \qquad \mu_{m,\,t} = \frac{\rho_m C_\mu k^2}{\varepsilon} \qquad (2)$$

In the present work, the density of each constituent is taken as constant. Equations 1 represent transport/generation of mixture volume, mixture momentum, and liquid phase volume fraction respectively. Physical time derivatives are included for transient computations. The formulation incorporates pre-conditioned *pseudo*-time-derivatives ($\partial/\partial\tau$ terms), defined by parame-

ter β, which provide favorable convergence characteristics for steady state and transient computations, as discussed in [7].

The formation and collapse of a cavity is modeled as a phase transformation. Mass transfer is modeled as finite rate interfacial processes:

$$\dot{m}^- = \frac{C_{dest}\rho_l\alpha_l \mathrm{MIN}[0, p - p_v]}{(1/2\rho_l U_\infty^2)t_\infty}$$
$$\dot{m}^+ = \frac{C_{prod}\rho_l\alpha_l^2(1-\alpha_l)}{t_\infty} \quad (3)$$

where $\dot{m}^-$ and $\dot{m}^+$ represent evaporation and condensation respectively. C_{dest} and C_{prod} are model constants ($C_{dest} = 100$, $C_{prod} = 1000$) obtained through experience and validation studies summarized in [6], [9]. A high Reynolds number form k-ε model with standard wall functions is implemented to provide turbulence closure. Further details on the physical modeling are provided in [6], [8].

Numerical Method

The numerical method is evolved from the work of Taylor and his coworkers ([14], for example). The UNCLE code which served as the baseline platform for the present work, is based on a single phase, finite volume, pseudocompressibility formulation. Third-order Roe-based flux difference splitting is utilized for convection term discretization. An implicit procedure is adopted with inviscid and viscous flux Jacobians approximated numerically. A block-symmetric Gauss-Seidel iteration is employed to solve the approximate Newton system at each pseudo-timestep.

The multi-phase extension of the code, designated UNCLE-M, retains these underlying numerics but incorporates additional volume fraction transport and mass transfer, non-diagonal preconditioning, and flux limiting. A temporally second-order accurate dual-time scheme is implemented for physical transients. The turbulence transport equations are solved subsequent to the mean flow equations at each pseudo-time step. The multiblock code is instrumented with MPI for parallel execution based on domain decomposition. Further details on the numerical method and code are available in [7].

4 Previous Applications, Validation Status and Analysis Requirements

UNCLE-M has been extensively used and validated for natural and ventilated sheet- and super-cavitation about external flow configurations. Of particular relevance here is that the code has been shown to predict bubble size parameters, drag and vapor/vorticity shedding characteristics for natural cavitation about numerous axisymmetric configurations with good accuracy [6 - 9].

Also important is our finding that such analyses require significantly higher discretization fidelity compared to single phase analyses. Specifically, finer wall normal and streamwise grid resolution, as well as higher order flux discretization (with attendant flux limiting) are required. Failure to accommodate these requirements results in: 1) a smearing of the vapor-liquid interface, especially near the aft end of the bubble (re-entrant flow region), 2) too small a cavity for a given cavitation number, and 3) steady-state results instead of the physically observed rich unsteady behavior (again, in particular, in the cavity re-entrant region).

5 Quasi-3D Analysis

The ultimate goal of this research is to establish a validated three-dimensional capability for the prediction of cavitation in pumps. As discussed above, accurate analysis requires significant grid resolution, accurate numerics and often a time-accurate solution strategy. Therefore, as we evolve our capability in this area, we have first pursued Q3D modeling wherein a nominal midspan blade-to-blade streamsheet is analyzed. This level of modeling has been widely used in turbomachinery design and analysis for centrifugal machines ([5], [12], for example). In centrifugal pumps, quantitative efficiency and off-design head performance cannot be captured with high accuracy since 3D effects including secondary flows are not incorporated. However, Q3D methods are usefully and widely employed in design and assessment studies.

The fully-three-dimensional relative frame code is adapted to perform Q3D analysis as follows: A throughflow design code developed by the fifth author is used to determine meridional streamsheets through the pump. Two nominally midspan streamsheets are extracted and imported into GRIDGEN [3]. The intersection of these streamsheets and the 3-D blade is determined within GRIDGEN and a structured multiblock grid is built bounded by the streamsheets and the blade intersection boundaries. An O-block is wrapped around the blade and multiple H-blocks are employed to retain good grid orthogonality and load balancing.

Two layers of cells are used in the spanwise direction (i.e., three vertex planes) so that second order accuracy can be retained for convection fluxes. A slip surface boundary condition is imposed on the upper and lower surfaces of the computational domain. Since these surfaces are defined as streamsheets, transport fluxes across these boundaries are set to zero and pressure on these boundaries is determined explicitly from a discrete approximation to the momentum equation dotted into the stream sheet surface normal.

For the single passage Q3D analyses presented in this paper, an 8 block, 36,288 vertex mesh was employed (12,096 vertices on each of the three spanwise planes). The calculations were carried out on several different computer systems using 8 processors in each case.

6 Test Case Considered

The pump analyzed was tested at the Pennsylvania State University Applied Research Laboratory, in the 12” water tunnel reconfigured as a pump test facility [11]. The performance of a backswept 7-blade impeller was tested at a variety of single phase and cavitating operating conditions. A photograph of the 7-blade impeller analyzed computationally here, is illustrated in the pump loop during installation in Figure 1.

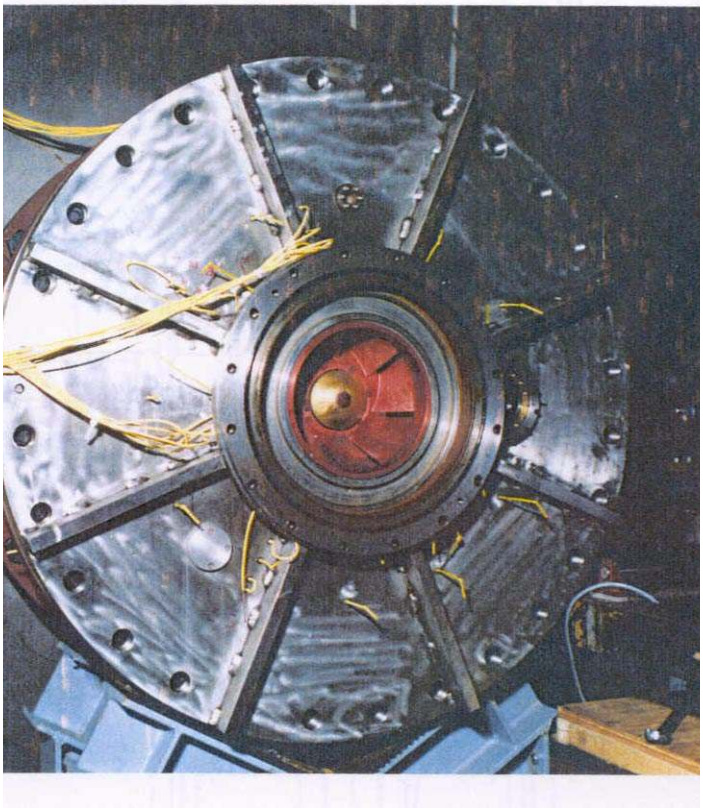

Figure 1. Photograph of 7-blade impeller during installation in the pump loop facility. Machine rotation is clockwise.

Figure 2 shows several video frames of this impeller operating at design flow coefficient, at successively lower cavitation numbers (optical access obtained through a prism mounted externally on viewing windows upstream of impeller). Clearly identified in these figures is a growing sheet cavity on the suction surface, that increases in length with span and extends onto the shroud. The approximate locations of the cavity trailing edge at midspan are indicated in the figure.

7 Results and Discussion

Quasi-Three-Dimensional Results

A total of 97 Q3D runs were performed covering operating conditions which span $0.4 \le \phi/\phi_{design} \le 1.5$, $0.099 \le \sigma \le 1.512$. Steady state solutions were obtained for most of the cases, but for cases run at low cavitation number and/or low flow coefficient, large sheet cavities develop and large scale unsteadiness is predicted near the aft end of these structures (re-entrant jet region). For these cases, the steady state runs do not converge but are used to initialize a time accurate simulation. In these cases, reported performance parameters are time-averaged quantities as illustrated in Figure 3.

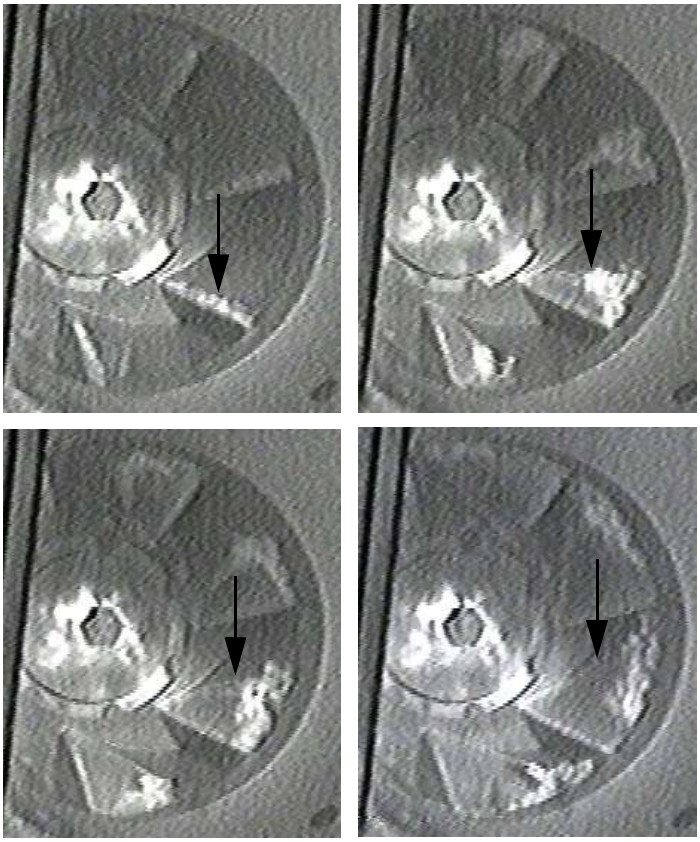

Figure 2. Video frames of 7-blade impeller during design flow coefficient operation at successively lower cavitation numbers. Approximate midspan cavity trailing edge location is indicated. Machine rotation is clockwise.

In what follows, four parameters are used to define the operating point and performance of the pump. These are the cavitation number, flow coefficient, head coefficient and efficiency, which are defined here as:

$$\sigma \equiv (p_\infty - p_v)/\frac{1}{2}\rho_l V_{ref}^2 \tag{4}$$

$$\phi \equiv V_{x,\,inlet}/U_{tip} \tag{5}$$

$$\psi \equiv \left[\left(\frac{\int p(\vec{v}\cdot d\vec{A})}{\int(\vec{v}\cdot d\vec{A})}\right)_{outlet} - \left(\frac{\int p(\vec{v}\cdot d\vec{A})}{\int(\vec{v}\cdot d\vec{A})}\right)_{inlet}\right]/\rho_l V_{ref}^2 \tag{6}$$

$$\eta = \frac{(\int p(\vec{v}\cdot d\vec{A}))_{outlet} - (\int p(\vec{v}\cdot d\vec{A}))_{inlet}}{\vec{\omega}\cdot\vec{T}} \tag{7}$$

where $(\vec{v} \cdot d\vec{A})$ is the mass flux through nominal impeller inlet and outlet computational planes and $\vec{T}$ is the total torque exerted on the fluid by the blade through pressure and viscous forces. The reference pressure, p_∞, is taken as that measured or computed upstream of the impeller in the entrance pipe section of the pump loop. (Note that static pressure is used in the head and efficiency definitions to conform to experimental measurements). For all of the computations carried out here, the flow coefficient is specified, that is, inlet velocity and machine rotation rate are input parameters. The implications of this on cavitation breakdown predictions is discussed below.

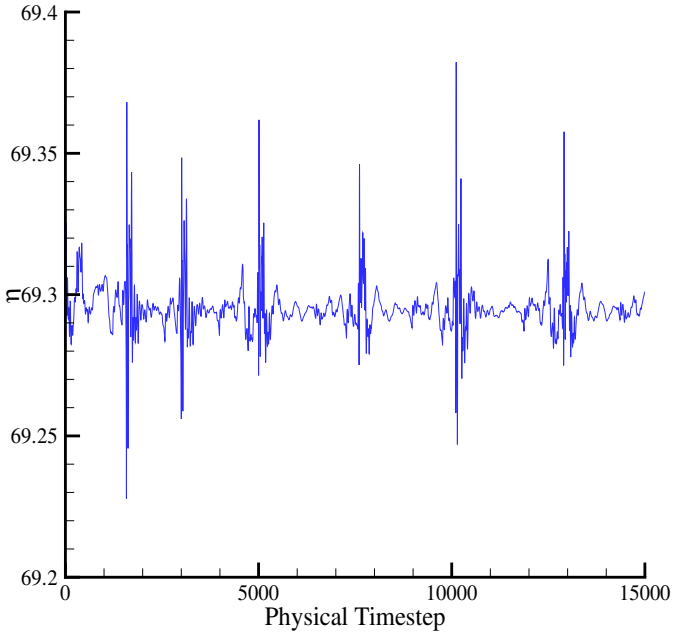

Figure 3. Efficiency vs. physical timestep for transient analysis, ϕ/ϕ_{design} = 1.0, σ = 0.200, $\Delta t/t_\infty$ = 0.002, average η = 69.29.

In Figure 4, single phase experimental and computational performance curves are presented for the impeller. Despite the Q3D nature of the analysis and the attendant difficulty in defining consistent pressure values between experiment and computation, predicted head coefficient and efficiency vs. flow coefficient compare reasonably well.

Figure 5 illustrates the general nature of the multiphase Q3D analyses. There, predicted streamlines and volume fraction contours are plotted for ϕ/ϕ_{design} = 0.8, at three cavitation numbers, σ = 0.547, 0.238, and 0.154, which correspond to incipient, developed and near-breakdown cavitation numbers for this case. Clearly observed in these plots is the development of a cavitation bubble on the suction surface, which increases in size as the cavitation number is decreased. At low cavitation number, a reentrant flow is observed near the cavity trailing edge, and some pressure surface cavitation is evident as well.

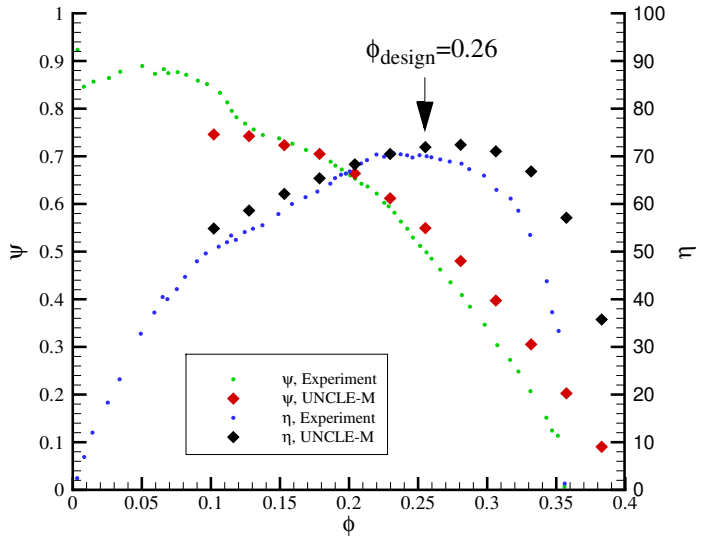

Figure 4. Comparison of experimental and computational head coefficient and efficiency vs. flow coefficient.

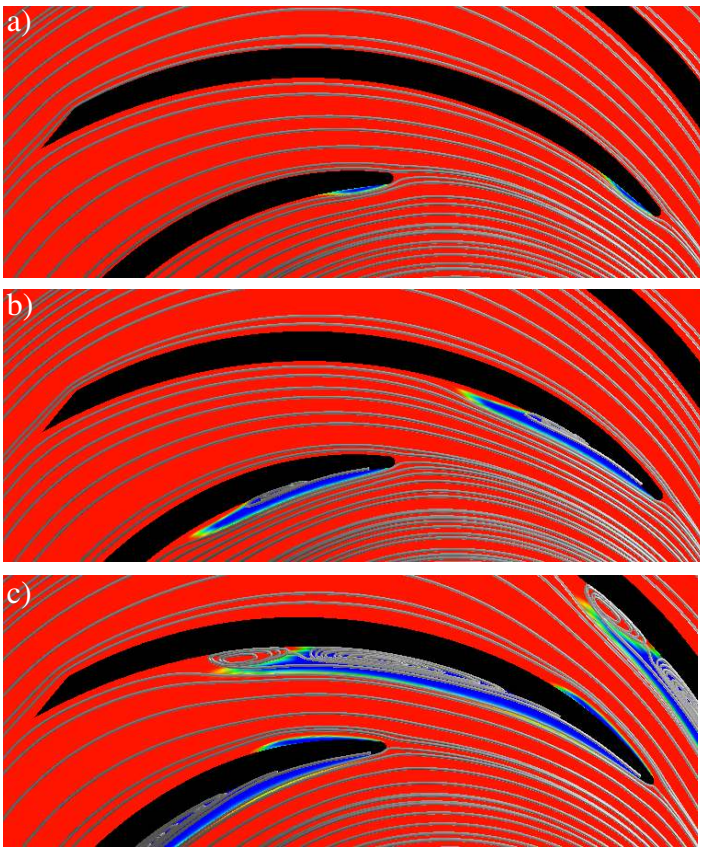

Figure 5. Streamlines and contours of volume fraction for ϕ/ϕ_{design} = 0.8. a) σ = 0.547, b) σ = 0.238, c) σ = 0.154. Machine rotation is clockwise.

Figures 6 through 8 show predicted cavitating performance curves. In Figure 6 hydraulic efficiency is plotted vs. flow coefficient for a range of flow coefficients, $0.4 \le \phi/\phi_{design} \le 1.5$. For each flow coefficient, a single phase calculation was performed. The inception cavitation number is then computed from equation 4 setting p_v to the minimum single phase pressure on the blade. From there, the cavitation number, which is an input parameter to the code, is successively lowered and the code rerun (time accurately if required as discussed above). This process was repeated at each flow coefficient until significant performance degradation was observed. As seen in the figure, the CFD analysis returns efficiency levels of up to twenty points lower than for single phase.

In Figure 7 head coefficient is plotted vs. flow coefficient for the same range of flow coefficients and cavitation numbers. Again, very significant head deterioration is returned by the code for low cavitation numbers, especially at off-design flow. In order to interpret these results more clearly, the same data is plotted as head coefficient vs. cavitation number in Figure 8. There it is seen that for each operating flow coefficient a critical cavitation number is reached below which the head coefficient drops dramatically with further reduction in cavitation number. This figure exhibits the familiar appearance of cavitation breakdown trends. Figure 9 shows a comparison of experimental and computed head coefficient vs. cavitation number at design flow coefficient. Though quantitatively overpredicting single phase head, due most likely to the Q3D nature of the analysis, the cavitation breakdown number and the "suddenness" of the drop-off is captured. From the qualitatively correct trends observed in Figure 8 and the reasonable quantitative comparison observed in Figure 9, it is concluded that the analysis is indeed capturing principal physical elements of cavitation breakdown.

To pursue this further we examine some local flow field solution plots. Figure 10 shows elements of two low flow ($\phi/\phi_{design} = 0.5$) simulations with significant cavitation. In Figure 10a, predicted streamlines and liquid volume fraction contours are presented for cavitation numbers of $\sigma = 0.110$ and 0.099, which correspond to operating conditions just before and well into predicted cavitation breakdown ($\psi = 0.739$ and 0.586 respectively in Figure 8). Just before breakdown a significant two-phase region is observed on the suction side, with an attendant large recirculation (re-entrant jet) at the aft end of the bubble. As the cavitation number is lowered only slightly more ($\Delta\sigma = .011$), the bubble grows explosively, blocking more than half of the passage. Figures 10b and c illustrate the significant decrease in passage pressure rise and significant increase in local relative velocity magnitude associated with this near-choking condition.

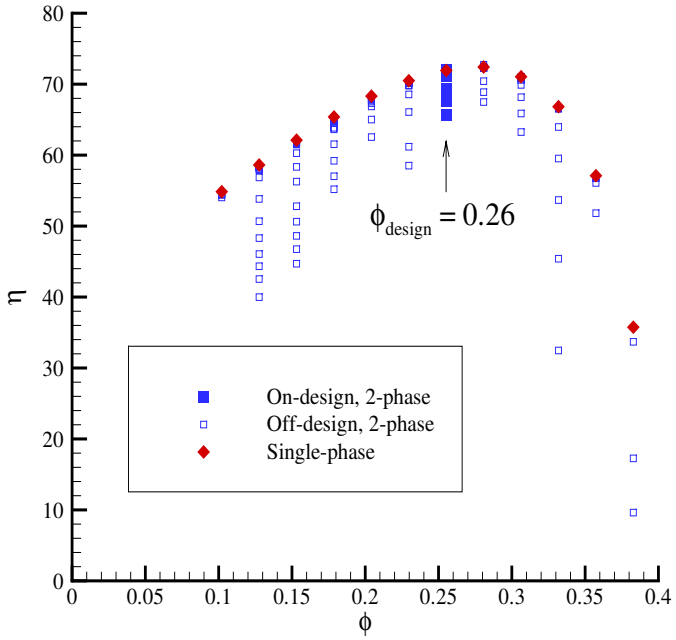

Figure 6. Predicted efficiency vs. flow coefficient for single-phase and multi-phase analyses.

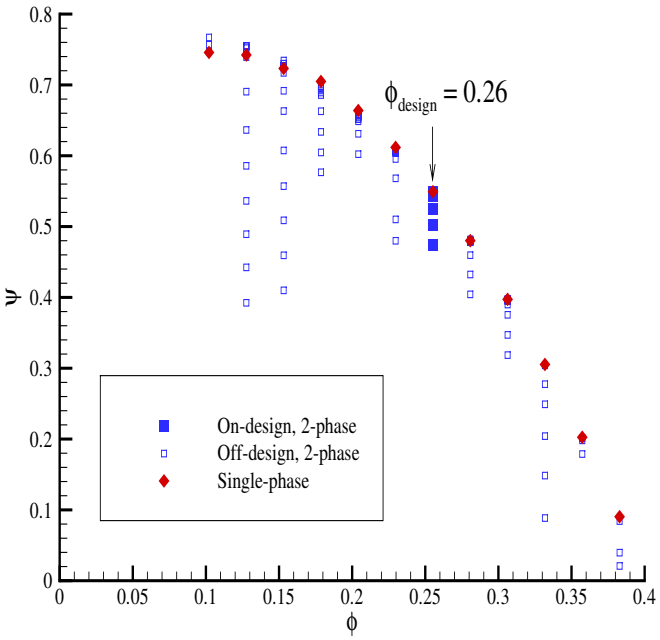

Figure 7. Predicted head coefficient vs. flow coefficient for single-phase and multi-phase analyses.

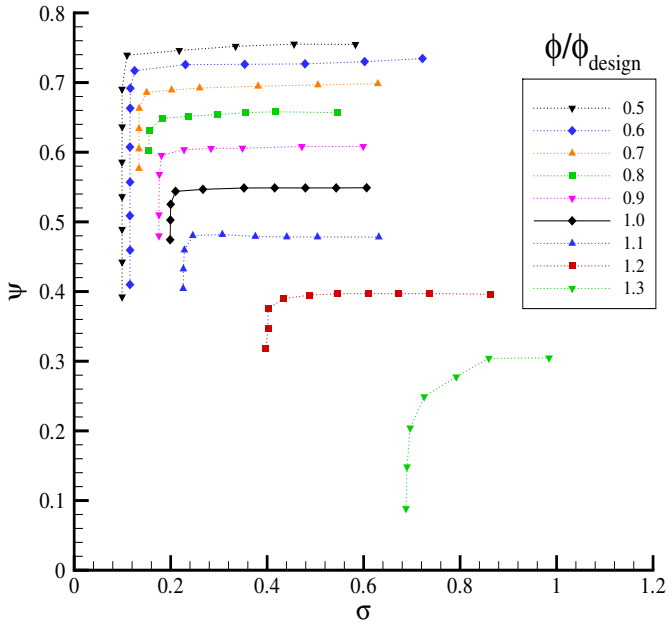

Figure 8. Predicted head coefficient vs. cavitation number for various non-dimensional flow coefficients.

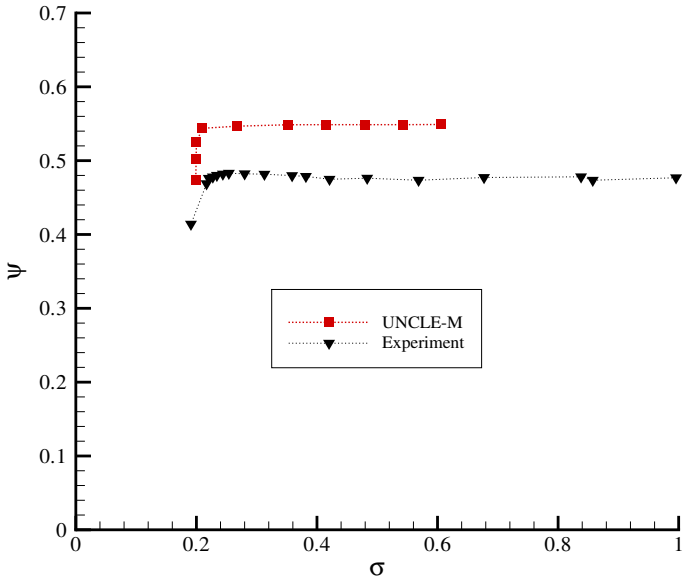

Figure 9. Numerical results vs. experimental results of head coefficient vs. cavitation number at design flow coefficient.

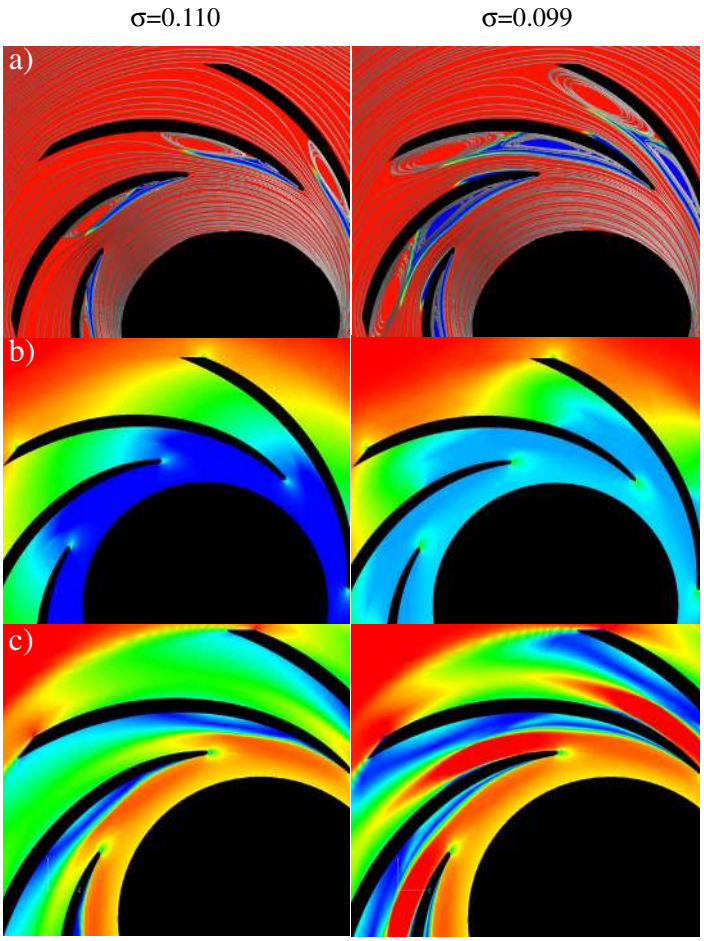

Figure 10. Predicted field variables for $\phi/\phi_{design} = 0.5$, $\sigma = 0.110$ and 0.099. a) volume fraction contours and streamlines, b) pressure contours, c) relative velocity magnitude contours. Machine rotation is clockwise.

Although these plots elucidate the principal physical mechanisms associated with the *onset* of cavitation breakdown, they should not be over-interpreted. In pumping systems, the operating point for the pump is defined by the intersection of the pump head-flow characteristic (which is a function of cavitation number) and the pump loop or pumping system characteristic (which is generally fixed). If the pump begins to cavitate significantly, both head rise *and flow rate* will drop. Well into breakdown, the resulting system dynamics can be highly unsteady, and these dynamics are not captured here since flow coefficient is a fixed parameter. In the future we plan to incorporate a quasi-steady analysis of the pump coupled with the system which should predict a change in the flow rate as well.

A final representation of the multiphase Q3D simulations is provided in Figure 11. There, inception (defined for the mass transfer modeling employed here from equation 4 with p_v set to the minimum single phase pressure on the blade) and breakdown

cavitation numbers are plotted vs. flow coefficient. Again standard trends for these parameters are observed.

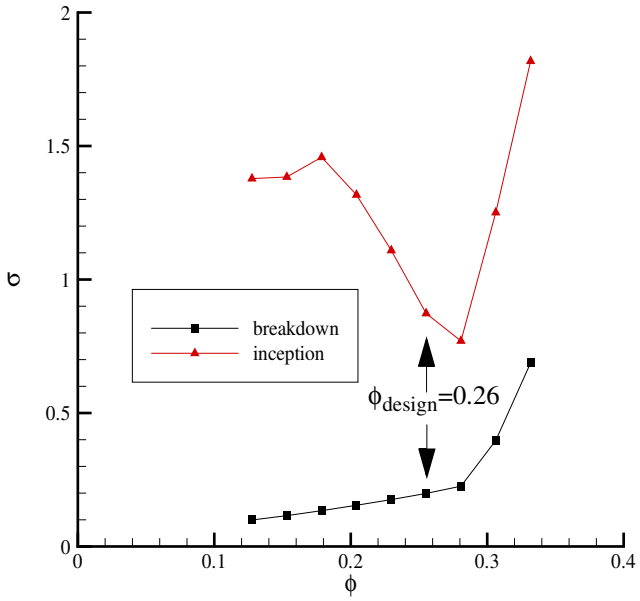

Figure 11. Predicted cavitation inception and breakdown points vs. flow coefficient.

Three-dimensional Results

The foregoing Q3D analyses demonstrate the capability of the method in capturing the physical mechanisms associated with sheet cavitation in centrifugal pumps. As mentioned above, we are maturing this work towards a reliable and validated full 3D time-dependent methodology. Current 3D capability is demonstrated here. Figures 12a and b show a front view of a notional shrouded impeller similar to the 7-blade impeller analyzed above and depicted in Figures 1 and 2. A 55,195 vertex grid was used for the single passage analysis. This grid is significantly coarser than the more than 500,000 nodes that we estimate would be required to get mesh independent cavitating results. A steady relative frame solution was obtained for this configuration at a range of cavitation numbers. The figures illustrate predicted blade surface and hub pressure contours and the predicted cavities (designated by a liquid volume fraction, $\alpha_l = 0.95$ isosurface) for two cavitation numbers. The predicted cavities exhibit similar features to those depicted in Figure 2. Specifically, at this design flow coefficient, cavitation is initiated near the leading edge on the suction surface. At low cavitation number the cavities exhibit significant three-dimensionality, with the streamwise extent of the cavity increasing with span. The bubble extends onto the shroud as well.

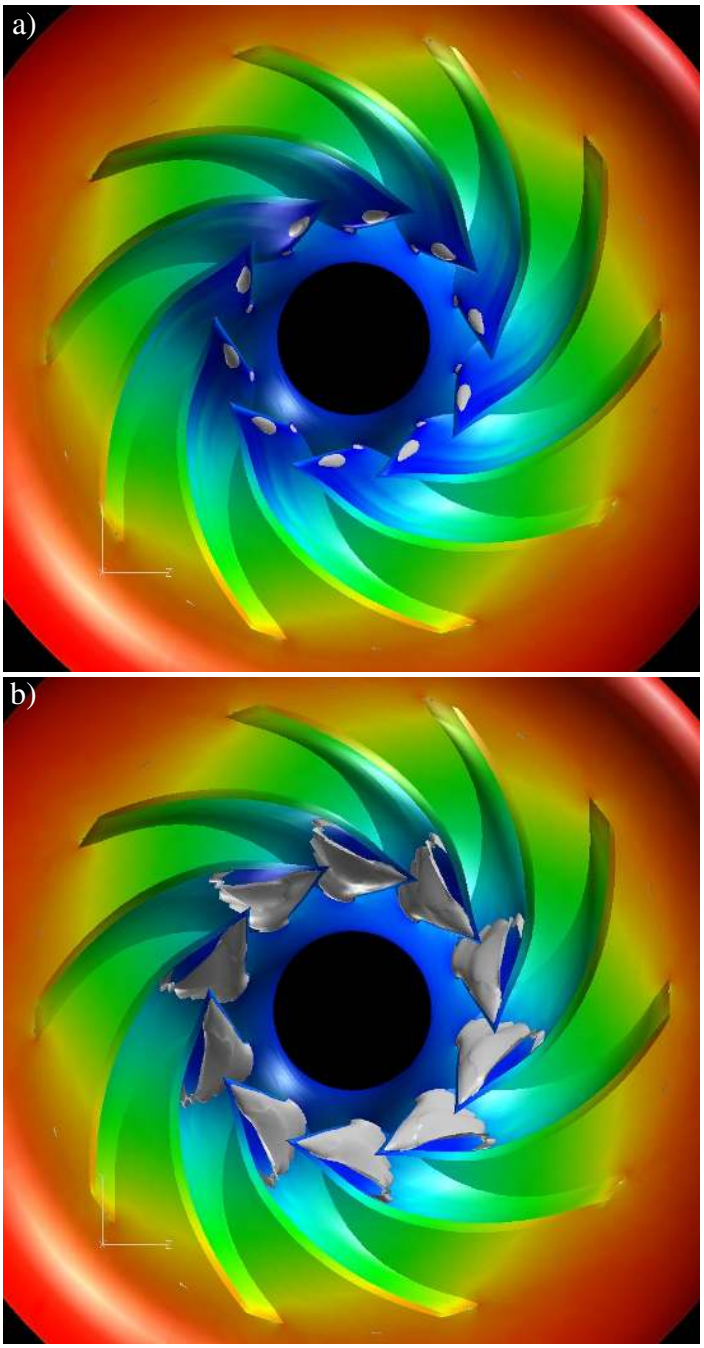

Figure 12. Front views of three-dimensional impeller simulation. Blade surface and hub pressure contours with cavity designated by liquid volume fraction, $\alpha_l = 0.95$ isosurface.
a) $\sigma = 0.40$, b) $\sigma = 0.28$

8 Conclusion

A homogeneous multi-phase CFD method was applied to analyze centrifugal pump flow under developed cavitating conditions. Quasi-three-dimensional analysis was used to model a 7-blade pump impeller across a wide range of flow coefficients and cavitation numbers. Performance trends associated with off-design flow and blade cavitation, including breakdown, are observed that compare qualitatively with experimental measurements. Local flow field solution plots were presented that elucidate the principal physical mechanisms associated with the onset of breakdown. Results were also presented that illustrate the full three dimensional capability of the method.

As this work continues the authors are pursuing improvements to three elements of the method including: 1) adapting mass transfer models, equation 3, to accommodate thermal effects on cavitation breakdown, 2) implementing time-varying pressure and mass flow boundary conditions that accommodate pumping system dynamics and 3) maturing/validating fully three-dimensional capability.

9 Acknowledgments

The first author's thesis program was supported under an Exploratory and Foundational program scholarship at the Pennsylvania State University Applied Research Laboratory. This work was supported in part by a grant of HPC resources from the Arctic Region Supercomputing Center and in part by a grant of SGI Origin 2000 HPC time from the DoD HPC Center, Army Research Laboratory Major Shared Resource Center.

10 References

1. Ahuja, V., Hosangadi, A., Ungewitter, R. and Dash, S. M., ''A Hybrid Unstructured Mesh Solver for Multi-Fluid Mixtures,'' AIAA 99-3330, 14th Computational Fluid Dynamics Conference, Norfolk, VA, June, 1999.
2. Chen, Y., Heister, S.D. (1994) "Two-Phase Modeling of Cavitated Flows," ASME FED-Vol. 190, pp.299-307.
3. Gridgen User Manual, Version 13.3, Pointwise, 1999.
4. Hirschi, R., Dupont, Ph., Avellan, F., Favre, J.-N., Guelich, J.-F., Parkinson, E. (1998) "Centrifugal Pump Performance Drop Due to Leading Edge Cavitation: Numerical Predictions Compared With Model Tests," *ASME Journal of Fluids Engineering*, Vol. 120, No. 4, pp. 705-711,
5. Jorgenson, P.C.E., Chima, R.V. (1989) "Explicit Runge-Kutta Method for Unsteady Rotor-Stator Interaction," *AIAA Journal*, Vol. 27, No. 6, pp. 743-749.
6. Kunz, R.F., Boger, D.A., Stinebring, D.R., Chyczewski, T.S., Gibeling, H.J., Govindan, T.R. (1999) "Multi-phase CFD Analysis of Natural and Ventilated Cavitation About Submerged Bodies," ASME Paper FEDSM99-7364.
7. Kunz, R.F., Boger, D.A., Stinebring, D.R., Chyczewski, T.S., Lindau, J.W., Gibeling, H.J., Venkateswaran, S., Govindan, T.R. (2000) "A Preconditioned Navier-Stokes Method for Two-Phase Flows with Application to Cavitation Predication," *Computers and Fluids*, Vol. 29, No. 8, pp. 849-875.
8. Kunz, R.F., Lindau, J.W., Billet, M.L., Stinebring, D.R. (2001) "Multiphase CFD Modeling of Developed and Supercavitating Flows," VKI Special Course on Supercavitating Flows, February.
9. Lindau, J.W., Kunz, R.F., Gibeling, H.J. (2000) "Validation of High Reynolds Number, Unsteady Multi-Phase CFD Modeling for Naval Applications," presented at the 23rd Symposium on Naval Hydrodynamics, Val de Reuil, France.
10. Merkle, C.L., Feng, J.Z. and Buelow, P.E.O. (1998) ''Computational Modeling of the Dynamics of Sheet Cavitation,'' 3rd International Symposium on Cavitation, Grenoble, France.
11. Meyer, R.S., Yocum, A.M. (1993) "Pump Impeller Performance Evaluation Tests for a Parametric Variation of Geometric Variables," ARL Technical Memorandum 93-125.
12. Nakamura, S., Ding, W., Yano, K. (1998) "A 2.5D Single Passage CFD Model for Centrifugal Pumps," ASME Paper FEDSM98-4858.
13. Song, C., He, J. (1998) "Numerical Simulation of Cavitating Flows by Single-phase Flow Approach," 3rd International Symposium on Cavitation, Grenoble, France.
14. Taylor, L.K., Arabshahi, A., Whitfield, D.L. (1995) "Unsteady Three-Dimensional Incompressible Navier-Stokes Computations for a Prolate Spheroid Undergoing Time-Dependent Maneuvers," AIAA Paper 95-0313.